A Lattice Boltzmann single component model for simulation of the autogenous self-healing caused by further hydration in cementitious material at mesoscale

Chen, Jiayi; Ye, Guang

DOI
10.1016/j.cemconres.2019.105782

Publication date
2019

Document Version
Final published version

Published in
Cement and Concrete Research

Cement and Concrete Research 123 (2019) 105782

Contents lists available at ScienceDirect

Cement and Concrete Research

journal homepage: www.elsevier.com/locate/cemconres

A Lattice Boltzmann single component model for simulation of the autogenous self-healing caused by further hydration in cementitious material at mesoscale

Jiayi Chen*, Guang Ye

Delft University of Technology, Delft, the Netherlands

ARTICLE INFO

Keywords:
Autogenous self-healing
Further hydration
Lattice Boltzmann Method
Nucleation probability distribution
Geometry change

ABSTRACT

Cracking is inevitable during the service period of concrete structures. They are preferential ingression channels for aggressive ions. It is difficult or even impossible to repair all the cracks due to the limitation of practical conditions. However, cracks have potentials to self-heal due to further hydration and carbonization. The effect of autogenous self-healing on the properties of cementitious materials has been studied experimentally by many researchers. However, researches on modelling of the autogenous self-healing processes are still limited. In this paper, a Lattice Boltzmann single component model is proposed to simulate the self-healing caused by further hydration in cement paste matrix at mesoscale. The model simulates not only the healing efficiency but also the geometry change. The simulation result shows that even when the filling efficiency is low, some locations in the crack could be completely blocked. This may lead to lower effective diffusion coefficient of ions via the cracked sample.

1. Introduction

Concrete is the most widely used man-made material, but cracking is inevitable during the service period of concrete structures. Cracks are preferential ingression channels for aggressive ions, e.g., chloride, sulphate, etc., which accelerate the degradation of concrete. The repair of cracks is difficult or even impossible to be executed due to the limitation of practical conditions. For instance, the location of damage may be not accessible in the damaged structure. Besides, many infrastructures such as highways and tunnels are in continuous service which makes repairing work very difficult. Even if such work were possible in principle, the cost and amount of labour required for diagnosis and repair works could be prohibitive, especially in the case of large-scale infrastructures [1].

Fortunately, cracks have potentials to self-heal due to the continuous hydration of unhydrated cement and carbonization [1-4]. The self-healing of cracks in fractured concrete was noticed by the French Academy of Science in 1836 already in water retaining structures, culverts and pipes [2]. The self-healing phenomenon was further studied by Hearn, Hyde and Smith [3, 5] at the end of the nineteenth century. A more systematic analysis of healing phenomena dates back to 1926 and was executed by Glanville [6].

Several possible causes can be responsible for the self-healing phenomena [7], which is described in Fig. 1 and explained as followed:

a. Formation of calcium carbonate or calcium hydroxide.
b. Blocking cracks by impurities in the water and loose concrete particles resulting from crack spalling.
c. Further hydration of the unreacted cement or cementitious materials.
d. Expansion of the hydrated cementitious matrix in the crack flanks (swelling of C-S-H due to water absorption).

Among these possible causes, the primary self-healing mechanism is attributed to further hydration and carbonization [1, 8], which is called autogenous self-healing.

The effect of autogenous self-healing on the properties of cementitious materials has been studied experimentally by many researchers [9-12]. However, modelling of the autogenous self-healing processes is still limited. The difficulty in the modelling of autogenous self-healing is that the healing process involve a series of chemical and physical processes, including dissolution of unhydrated cement particles, transport of dissolved ions and formation of hydration and carbonization product. It is difficult to mimic these complex processes precisely. Only a few numerical models were proposed to address this complicated issue [13-16].

* Corresponding author.
E-mail address: J.Chen-2@tudelft.nl (J. Chen).

https://doi.org/10.1016/j.cemconres.2019.105782
Received 23 October 2018; Received in revised form 14 April 2019; Accepted 4 June 2019
Available online 27 June 2019

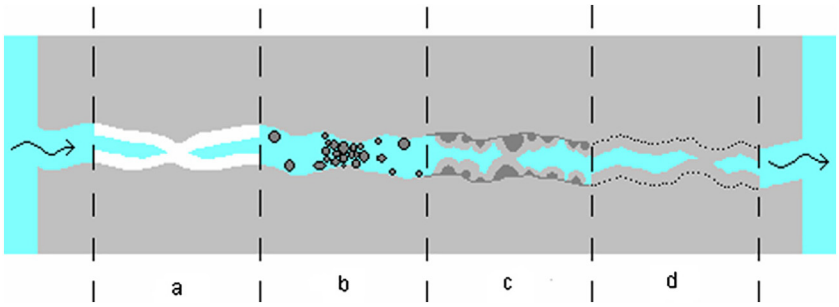

Fig. 1. Possible mechanisms for self-healing in cementitious materials [7].

Huang et al. [13, 14] proposed a reactive transport model, taking into account the particle distribution and further hydration of cement. In their model the microstructure formation of cement paste was simulated by existing hydration model [17]; the diffusion and thermodynamic laws were applied to simulate the healing process by implementing Fick's second law and employing the geo-chemical model JCHESS [18]. The calculated result of filling fraction by the healing products in microcracks was in good agreement with their experimental results.

A coupled thermo-hygro-chemical model was proposed by Chitez and Jefferson [15] to characterize the autogenous healing in ordinary cementitious materials. They concluded that the available database from existing geochemical systems cannot be used since it does not contain sufficient information for the relevant solids and aqueous species for the healing process of cementitious materials; therefore, the clinker was modelled as a single solute in the model. Their simulation results were also in good agreement with experimental data.

Aliko-Benitez et al. [16] proposed a chemical-diffusive model to simulate the self-healing behaviour in concrete, of which the healing mechanism of precipitation of calcium carbonate inside the cracks was proposed. The model simulated that CO_2 enriched water permeated through the specimen, and carbonate CO_3^{2-} reacted with the calcium ions Ca^{2+} embedded in the cement matrix, to produce precipitation of calcium carbonate to fill the void volume. The diffusion coefficients of ions in the matrix were assumed to be independent on the damage and healing process of cracking, and the damages were assumed to be uniformly distributed within the concrete structure.

From above mentioned models, most researchers implicitly assumed that the filling product was evenly distributed along the crack. This assumption is reasonable when the crack width is small, so the crack can be completely healed. However, the filling mechanism will play a vital role when the crack can not be healed completely. According to [19], the assumption is invalid in this case: some locations of the crack is blocked completely, even though the total volume of hydration product is quite limited. The influences of autogenous self-healing on the transport properties may be underestimated in existing studies. It is vital to simulate the autogenous self-healing of individual crack, so the influences of self-healing effect on the transport properties can be evaluated.

In this paper, a Lattice Boltzmann single component model is proposed to simulate the autogenous self-healing of the crack caused by further hydration in cement paste matrix at mesoscale. The model simulates not only the filling efficiency, but also the geometry change during the healing process. Simulation result shows that even when the filling efficiency is low, some locations in the crack could be completely blocked, as observed from experiments [19]. This may lead to the decrease of the effective diffusion coefficient of ions via the cracked sample.

2. Methodology

The simulation of autogenous self-healing is to mimic the physical and chemical processes of self-healing at mesoscale. The simulation focuses on mesoscale because that all hydration products contribute to the filling of crack. The phase of hydration products, such as calcium silicate hydrates (C-S-H) and potlandite (CH), were not separated in the simulation but identified as high density (HD) hydration product and low density (LD) hydration product. This also reduces the computational burdens in the simulation when the physical length of the crack reaches thousands micrometers.

The simulation flow chart is given in Fig. 2. The proposed model process consists of several aspects as follows. Firstly, the domain with crack is obtained from previous experiments [19] by image analysis. Secondly, the dissolution rates of individual cement particles are calculated according to [17]. Thirdly, the dissolved ions are transported in the domain simulated by using Lattice Boltzmann Method (LBM). Fourthly, the nucleus formation is simulated based on nucleation probability distribution. Lastly, the growth of nucleus is calculated according to the growth rate and the concentration of ions. Each cycle of the simulation includes dissolution, transport, nucleus formation and growth. All these steps will be explained in detail in the following sections.

2.1. Initialization

In the previous experiment [19], pre-cracked cement paste samples were monitored under light microscope to quantify the effects of autogenous self-healing. The images from the experiment are used in this paper as input to simulate the self-healing processes and to validate the model. A brief introduction of the experiment is given at following paragraphs.

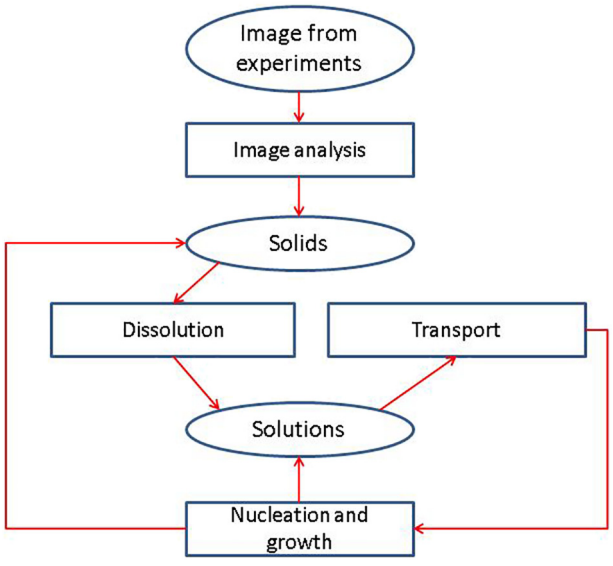

Fig. 2. The simulation flow chart.

Table 1
Chemical composition of CEM I 42.5N.

	CaO	SiO_2	Fe_2O_3	Al_2O_3	MgO	Na_2O	K_2O	CuO
Composition (% wt)	64.99	17.11	3.59	3.8	1.56	0	0.16	0.02
	ZnO	P_2O_5	TiO_2	Cl	SO_3	*Other*	*LOI* (550 °C)	*LOI* (950 °C)
Composition (% wt)	0.15	0.63	0.27	0.02	3.96	2.01	1.64	3.1

Table 2
The information of sample.

Sample	w/c ratio	Age (days)	Average crack width (μm)
A30S07W15	0.30	7	15

2.1.1. Materials and sample preparation

The cement paste samples were casted with Portland cement CEM I 42.5N. The chemical composition of cement is given in Table 1. The information of the sample is given in Table 2. The hydration degree is about 77.4%, which is approximated from [17].

The experiment was carried out with following procedure:

- the cement paste was casted and cured under sealed condition at room temperature;
- the thin-section of cement paste with the thickness of 100 ± 10 μm was made by cutting, grounding and polishing with ethanol;
- the thin-section was cracked under light microscope to obtain desired crack width;
- the cracked thin-section was glued on the glass to maintain the stability of the crack;
- the sample was saturated with deionized water and sealed immediately to avoid carbonization;
- the autogenous self-healing process was monitored under light microscope continuously;
- both images under the polarized filter and under the crossed polarized filters were taken to carry out petrographic analysis.

2.1.2. Image analysis

The image, shown in Fig. 3a, was taken from the experiment under the polarized filter. The resolution is 0.433 μm/pixel. It is analyzed to obtain the simulation domain, representing the initial state before self-healing.

Image segmentation is performed by using the threshold method, which is based on a threshold value of grey scale to turn a grayscale image into a binary image. Colour images can also be thresholded. One approach is to designate a separate threshold for each of the red green and blue (RGB) components of the image and then combine them with an AND operation. Both methods are used in this paper to segment the image into different phases, i.e., the crack, unhydrated cement, HD product and LD product.

The origin image shown in Fig. 3a is converted into grayscale image and segmented into different phases where the crack mask is given in Fig. 3b and unhydrated cement particles are shown in Fig. 3c. A few parameters can be calculated from these images.

For instance, the effective area A_{Eff} is the area before the cracking, which is defined in Eq. (1). Initial cement area A_{IC} and initial liquid area are the initial phases before the hydration. The gap between initial cement area A_{IC} and current unhydrated cement particles is the HD product [20]. Initial cement area A_{IC} and initial liquid area A_{IW} are calculated according to hydration degree D_H and water to cement ratio (*w/c ratio*) with Eqs. (2) and (3).

In the simulation, the solid phase consists of HD product, LD product and unhydrated cement. According to cement hydration model [17], the HD C-S-H will form in the place originally occupied by unhydrated cement. It is assumed that the space between the dissolution front and the original edge of the particle is HD product, given in Fig. 3d. The rest area of solid phase is LD product. The whole simulation domain is given in Fig. 3e, consisting of the crack, unhydrated cement, HD and LD product.

To reduce the computation burden, the concept of effective zone proposed by [21] is adapted in this study. The length L and width W of the effective zone are 842 μm and 211 μm, respectively. The effective zone is shown in Fig. 3f.

$$A_{Eff} = A_{Domain} - A_{Crack} \tag{1}$$

$$A_{IC} = \frac{A_{Un}}{1 - D_H} \tag{2}$$

$$w/c\ ratio = \frac{\rho_w \cdot A_{IW}}{\rho_c \cdot A_{IC}} \tag{3}$$

where:

- A_{Eff} is the effective area in the domain without crack
- A_{IC} and A_{IW} are areas of initial cement and water, respectively
- *w/c ratio* is water to cement ratio
- ρ_{water} and ρ_{cement} are densities of water and cement particle, respectively

2.2. Discretisation of space and time

Based on the image processing, the unit of the simulation domain L_0 is 0.433 μm. Each pixel in the image is considered as a node in Lattice Boltzmann model. The discretisation of time is carried out via unit conversion of Lattice Boltzmann (LB) with dimensionless parameter Fourier number F_o, with Eqs. (4) and (5). The relaxation time of LB is calculated with D_{HD}^{LB}, with Eq. (6).

$$F_o = \frac{Dt}{L^2} \tag{4}$$

$$\frac{D_{HD}^{P} t}{L^2} = F_o = \frac{D_{HD}^{LB} T}{L_{lb}^2} \tag{5}$$

$$D_{HD}^{LB} = \frac{1}{3}\left(\tau - \frac{1}{2}\right) \tag{6}$$

where:

- D is the diffusion coefficient (unit: m^2/s)
- t is the characteristic timescale(unit: s)
- L is the length scale of interest(unit: m)
- D_{HD}^{P} and D_{HD}^{LB} are the diffusion coefficient of ions in high density phases in reality and LB, respectively
- L_{LB} is the dimension length of the domain in LB
- τ is the relaxation time
- T is the total simulation cycles

The diffusion coefficients of single solute in HD and LD products and liquid are measured experimentally by [22] and [23], given in Table 3. Unhydrated cement is assumed to be impermeable.

2.3. Dissolution of unhydrated cement

The dissolution rate of unhydrated cement $k_{r,x}$ is calculated with Eq. (7), according to [17].

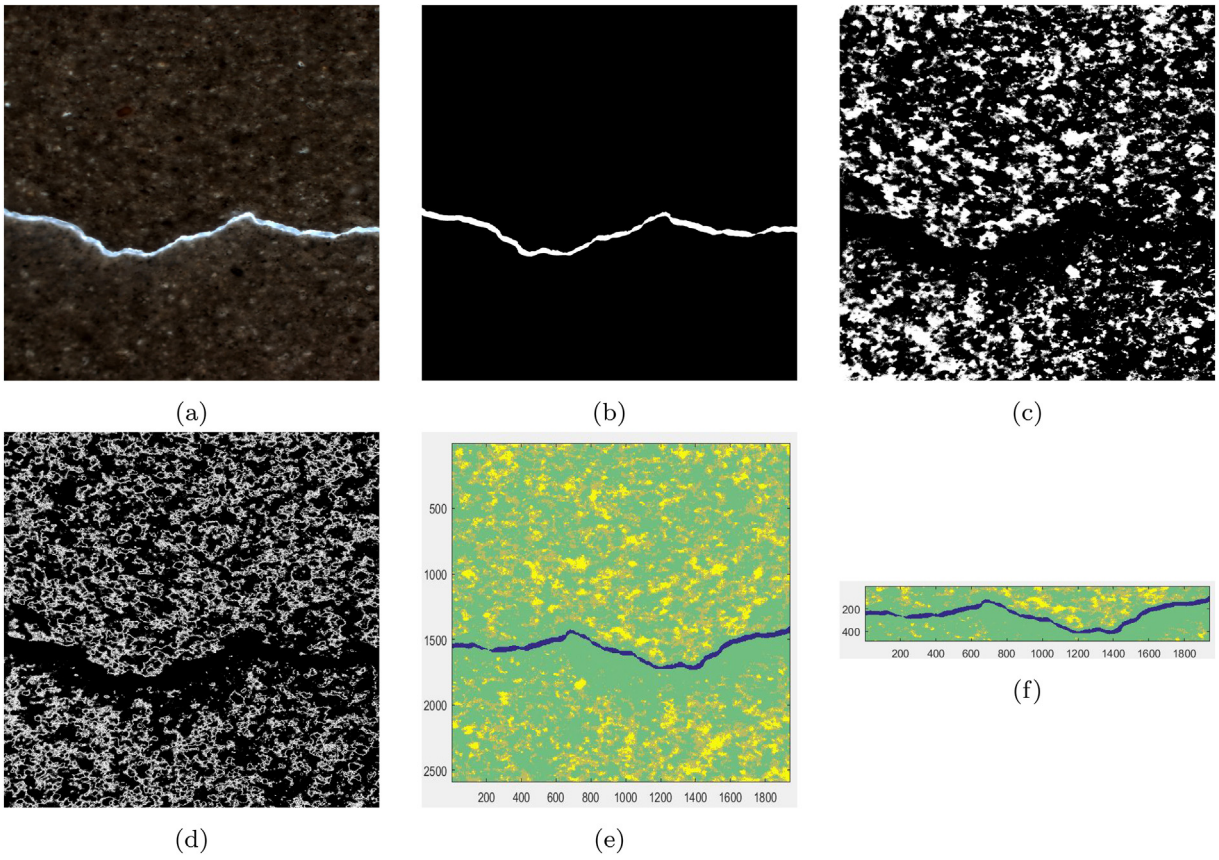

Fig. 3. Image process of the image taken during self-healing experiment: (a) Origin image; (b) crack pattern; (c) unhydrated cement; (d) HD product; (e) full domain; (f) final domain (effective zone).

$$k_{r,x} = k_0 \left(\frac{\delta_{tr}}{\delta_{t,x}} \right)^{\lambda} \tag{7}$$

The basic dissolution rate k_0 is 0.045μm/h, and the transition thickness δ_{tr} is 3.6 μm [17]. $\delta_{t,x}$ is the thickness between node x to nearest liquid node. λ equals to 0 when $\delta_{t,x}$ is smaller than δ_{tr}, otherwise it equals to 1.

It is assumed that the thickness of the domain is one unit length L_0, so L_0^2 is the area of node x. dt is the time incremental. $dv_{c,x}$ is the dissolution volume of cement at node x in the time incremental dt, calculated with Eq. (8).

$$dv_{c,x} = k_{r,x} L_0^2 dt \tag{8}$$

The HD product is assumed to form in the place originally occupied by unhydrated cement. The volume of HD product equals to the dissolved cement, given in Eq. (9).

$$dv_{HD,x} = dv_{c,x} \tag{9}$$

During the microstructure development of cement hydration, the volume of hydration products is about 2.2 time of the volume of hydrated cement, according to [20]. This implies that the total volume of HD and LD products is 2.2 times the counterpart of dissolved cement, given in Eq. (10).

$$dv_{HD,x} + dv_{LD,x} = 2.2 dv_{c,x} \tag{10}$$

It is assumed that the formation of HD product is at the same moment of dissolution of cement particle, so the mass of the solute is equal to the mass of potential LD product which will form later in the crack. The volume of potential LD product can be deduced from Eqs. (9) and (10), and the mass of solute $dm_{i,x}$ is deduced from Eq. (11).

$$dm_i = dm_{LD,x} = dv_{LD,x} {}^{*} \rho_{LD} \tag{11}$$

The solution field of the domain is updated by adding the mass of solute $dm_{i,x}$ to each node x.

2.4. Ions transport

Similar to the model proposed by [15], in this paper the dissolved cement is considered as a single solute. A single component LB node system is implemented to simulate the ions transport. For simplification, it is assumed that the domain is saturated with water during the simulation. Hereinafter,the diffusion coefficients are the effective coefficients of single solute in the phases under water-saturated condition, including liquid phase and porous media. The fluid flow is ignored, and the boundary of domain is periodic.

Table 3
Different phases in the simulation.

Phase	HD product	LD product	Unhydrated cement	Liquid
Diffusion coefficient (m^2/s)	1.0×10^{-12} [22]	9.0×10^{-12} [22]	–	7.2×10^{-10} [23]
Density(kg/m^3) [24]	2195	1850	3120	1000

2.4.1. Lattice Boltzmann Method

The ion transport can be described by the following lattice BGK equation:

$$f_i(x + e_i\delta_t, t + \delta_t) = f_i(x, t) - [f_i(x, t) - f_i^{eq}(C, u)]/\tau_x \quad (12)$$

where f_i is the distribution function of the solute concentration; δ_t is the time increment; τ_x is the relaxation time; C is the solute concentration; u is the velocity of fluid flow; e_i are the discrete velocities, and f_i^{eq} is the corresponding equilibrium distribution function. The nine-speed (D2Q9) model is used, which e_i have the following form:

$$e_i = \begin{cases} 0 & i = 1, \\ (\cos[(i-1)\pi/2, \sin[(i-1)\pi/2]]) & i = 1-4, \\ \sqrt{2}(\cos[(i-5)\pi/2 + \pi/4], \sin[(i-5)\pi/2 + \pi/4]) & i = 5-8, \end{cases} \quad (13)$$

The relaxation time τ_x is related to the diffusion coefficient D_x, so τ_x is calculated with Eq. (14).

$$D_x = (\tau_x - 1/2)/3 \quad (14)$$

The equilibrium distribution function f_i^{eq} has the following form:

$$f_i^{eq}(C, u) = w_i C[1 + 3e_i{\cdot}u + 4.5(e_i{\cdot}u)^2 - 1.5u^2] \quad (15)$$

Because the velocity u of the fluid flow is negligible in the self-healing process, following equation is yielded:

$$f_i^{eq}(C) = w_i C \quad (16)$$

where w_i is the associated weight coefficients, which

$$w_i = \begin{cases} 4/9 & i = 0, \\ 1/9 & i = 1-4, \\ 1/36 & i = 5-8, \end{cases} \quad (17)$$

The solute concentration is calculated with Eq. (18)

$$C(x, t + \delta_t) = \sum_i f_i(x, t + \delta_t) \quad (18)$$

2.4.2. Relaxation time

The effective diffusion coefficients of solute in different phases under water-saturated condition are varying. To take into account the influence of different features, e.g., capillary and gel pores, and microcracks, etc., diffusion coefficient for each node is assigned based on the phase type of the node. The relaxation time is related to diffusion coefficient with Eq. (14) in LB, so τ_x is assigned and updated according to phase type of the node with Eq. (19). This approach has been studied by many researchers [25-27].

$$\tau_x = \begin{cases} 3D_W^{LB} + 1/2 & \text{x is liquid node,} \\ 3D_{HD}^{LB} + 1/2 & \text{x is high density node,} \\ 3D_{LD}^{LB} + 1/2 & \text{x is low density node} \end{cases} \quad (19)$$

The diffusion coefficient of ions in high density product in Lattice Boltzmann simulation D_{HD}^{LB} is calculated according to unit conversion with Eq. (5), while the counterparts in LD product D_{LD}^{LB} and liquid D_W^{LB} at Lattice Boltzmann simulation are calculated based on their ratios with diffusion coefficient in HD product in reality with Eqs. (20) and (21).

$$D_{LD}^{LB} = D_{HD}^{LB}\frac{D_{LD}^P}{D_{HD}^P} \quad (20)$$

$$D_W^{LB} = D_{HD}^{LB}\frac{D_W^P}{D_{HD}^P} \quad (21)$$

where D_{LD}^P, D_{HD}^P and D_W^P are the effective diffusion coefficients of solute in LD and HD products and liquid, respectively; D_{LD}^{LB}, D_{HD}^{LB} and D_W^{LB} are their counterparts in LB simulation, respectively.

2.5. Boundary condition

The domain of interest is part of the whole sample, so a periodic boundary condition is applied for solute transport in the simulation.

2.6. Nucleation and growth of hydration product

According to classical nucleation theory, phase transformations in the region of metastability are initiated within the original phase by the nucleation of small regions of the new phase, which then grow to macroscopic dimensions. Nucleation is characterized by large amplitude fluctuations, which are localized and stochastic in both space and time [28].

Generally the fluctuation is taken to be a cluster of a few atoms or molecules in the configuration of the new phase. The probability that a fluctuation occurs is governed by thermodynamic conditions, specially the minimum work, i.e., the nucleation barrier, required to create the cluster. It is assumed that nucleus are formed independently, thus the probability of forming a nuclei in the solution can be calculated via nucleation probability distribution.

2.6.1. Nucleation probability distribution

When the appearance of nuclei is independent, the probability P_m of forming m nuclei in a time interval is described by the Poisson distribution [29].

$$P_m = \frac{N^m}{m!}\exp(-N) \quad (22)$$

The probability that at least 1 nuclei $P_{\geq 1}$ can be found in the solution equals to 1 minus the probability that no nuclei P_0 is formed at all. $P_{\geq 1}$ can be calculated with Eqs. (23)–(25).

$$P_{\geq 1} = 1 - P_0 = 1 - \exp(-N) \quad (23)$$

$$N = JVt \quad (24)$$

$$J(S) = AS\exp\left(-\frac{B}{\ln^2 S}\right) \quad (25)$$

where N is the average number of nuclei formed in time interval t; V is the volume of solution;J is the nucleation rate; S is the saturation degree; A and B are kinetic and thermodynamic parameters for nucleation, respectively.

$$N_t = \iint N_{x,t}\,dxdt \quad (26)$$

The location of nuclei formation is also important to simulate the self-healing process. To determine the location of newly formed nucleus, each node of LB is considered as individual solution, of which the probability is calculated individually. The total number of nucleus N_t formed at time t is the integral of $N_{x,t}$ over all nodes and the time with Eq. (26). $N_{x,t}$ is the number of average nucleus formed in solution of node x at time t. The location of newly formed nucleus (lattice node) is chosen randomly based on the probability of individual nodes.

2.6.2. Nucleation and growth parameters

Kinetic parameter A and thermodynamic parameter B for nucleation can be obtained via the experiment in [29]. Growth rate k_g can be measured via the experiment in [30]. Those parameters are the essential properties of material, thus they are constant values.

In this paper these parameters are determined through parameter studying.

3. Parameter studying

In this parameter study, the maximum saturation degree (*maxSD*), kinetic parameter A and growth rate k_g are explicitly determined. The *maxSD* is the upper limit of the saturation degree for the solution. Both

Table 4
The range of parameters.

Level	*maxSD* (Unit: 1)	*A* (Unit: $m^{-3}s^{-1}$)	*B* (Unit: 1)	k_g (Unit: $kg\,m^{-2}s^{-1}$)	Initial saturated
1	2.5	10^{12}	0.4	40	Yes
2	3	10^{13}		80	No
3				160	

kinetic parameter *A* and thermodynamic parameters *B* influence the nucleation rate, but *A* is dominant in Eq. (25). The impact of *B* is less significant and keep constant in this study.

The range of each parameter is given in Table 4. The combinations of different parameters are simulated. A few results are shown at following sections to demonstrate the influence of each parameter when other parameters are constant.

The dimension of LB domain is 1944 × 487, and the iterative cycles are 104,999. The average computational time is 23 h per simulation.

During the parameter studying, the healing pattern is given to show the location and growth of formed nucleus. Similar to the experiments [19], the statistic analysis of crack filling is then executed: the filling ratios are calculated along the crack, and the results are sorted and then grouped according to the filling efficiency, e.g., 0%, from 0% to 10%, etc.

3.1. The impacts of maximum saturation degree

The simulation results with two different *maxSD* (2.5 and 3.0) are shown in Fig. 4a and b, respectively. The results are compared with each other to study the impacts of *maxSD*, i.e., the upper limit of saturation degree. The healing product in the crack is highlighted in the images to distinguish existing crack edge and newly formed product. It is clear that the simulation with higher *maxSD* has more healing product in the crack space. Fig. 4c is the statistic analysis of healing effect: the x axis is the efficiency, the columns are the length of locations with these filling efficiencies divided by the total length of the crack in percentage. It is clear that when *maxSD* is greater, the length of crack with no healing product is also shorter. This is because that *maxSD* determines the ion reserved in the solution: higher saturation degree means higher concentration of solute. At the same healing time, the simulation with greater *maxSD* has higher number of nucleus, according to Eqs. (24) and (25), thus the formation of hydration product is faster.

3.2. The impacts of kinetic parameter A

The simulation results with different kinetic parameter *A* are given in Fig. 5. From Fig. 5a and b, the simulation with higher *A* shows greater number of nucleus and the hydration product is distributed more evenly along the crack when all other parameters are fixed. It can be observed from Fig. 5c, that the average size of the hydration product is smaller for the simulation with higher *A*, which indicates that the hydration product is more evenly distributed; therefore it is difficult to bridge the crack. The regaining of mechanical property is especially relied on the bridging of cracking. Further study is required to quantitatively investigate the properties regaining due to self-healing, e.g., in terms of mechanical and transport properties.

3.3. The impacts of growth parameter

The simulations with different growth rates are given in Fig. 6, and their other parameters are constant. With the same dissolution rate of cement and *maxSD*, the total mass of solute is at similar level for nucleation. The numbers of formed nucleus are also alike, based on Eqs. (24)–(26). From Fig. 6d it can be observed that the shapes of healing product distribution show good agreement with these observations. Meanwhile, the simulation with higher growth rates has shorter length of crack without any hydration product, i.e., the length of crack with 0% healing efficiency is shorter. But this effect is limited by the amount of ions available for growth. When the growth rate of the simulation is doubled from $k_g = 80$ to $k_g = 160$, the filling efficiency is not improved significantly.

3.4. The impacts of initial saturation condition

The simulations with different initial saturation conditions are given in Fig. 7. Fig. 7a is initialised with water, while Fig. 7b is initialised with saturated solution. The total healing efficiencies are 22.94% and 25.62%, respectively. The nucleation probability accumulates significantly when saturation degree increases and time elapses, based on Eqs. (23)–(25). When the simulation is initialised with saturation solution, it has greater number of nucleus at the beginning, compared to the counterpart of simulation initialised with pure water. This leads to higher rate of ions consumption and cement dissolution, thus higher healing efficiency.

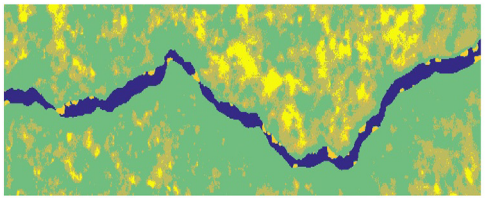

(a)

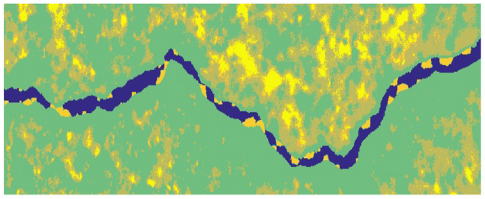

(b)

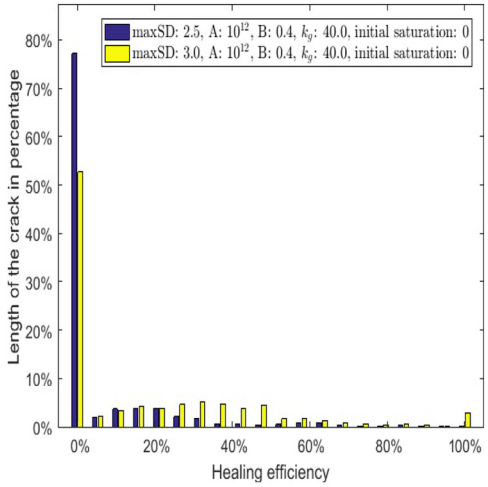

(c)

Fig. 4. The impacts of maximum saturation degree: (a) *maxSD* = 2.5, (b) *maxSD* = 3.0, (c) statistic analysis.

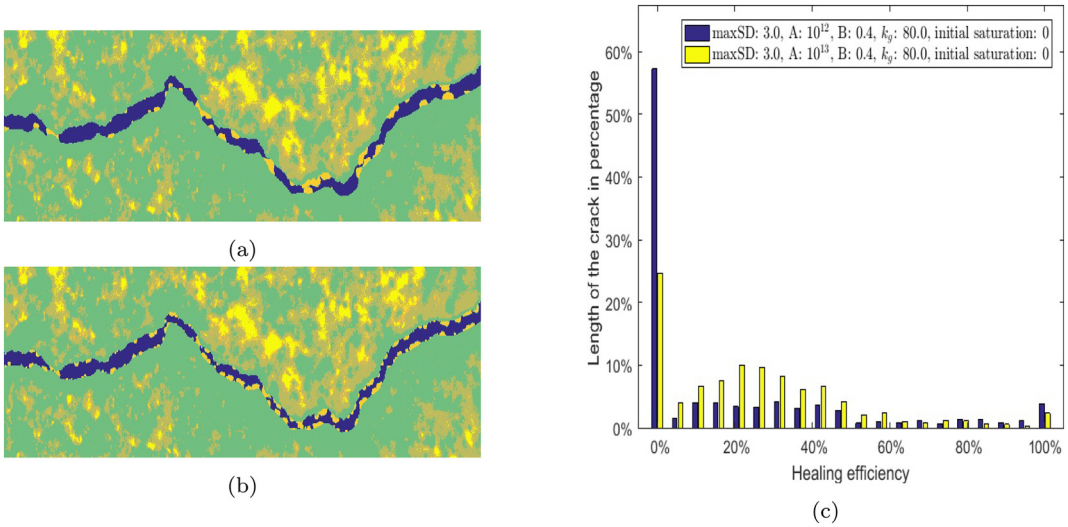

Fig. 5. The impacts of nucleation parameters: (a) $A = 10^{12}$, (b) $A = 10^{13}$, (c) statistic analysis.

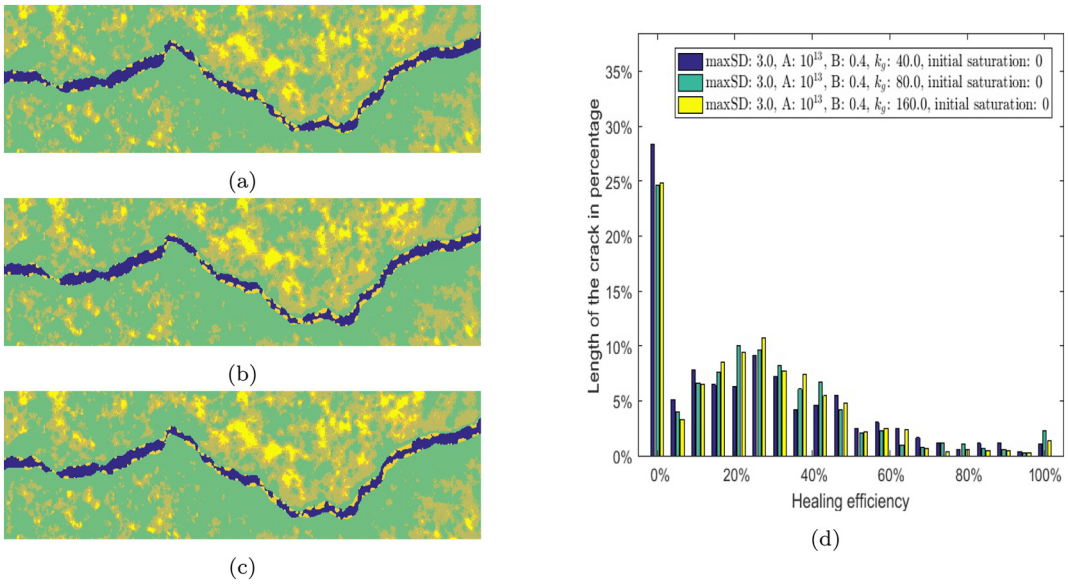

Fig. 6. The impacts of growth parameters: (a) $k_g = 40$, (b) $k_g = 80$, (c) $k_g = 160$, (d) statistic analysis.

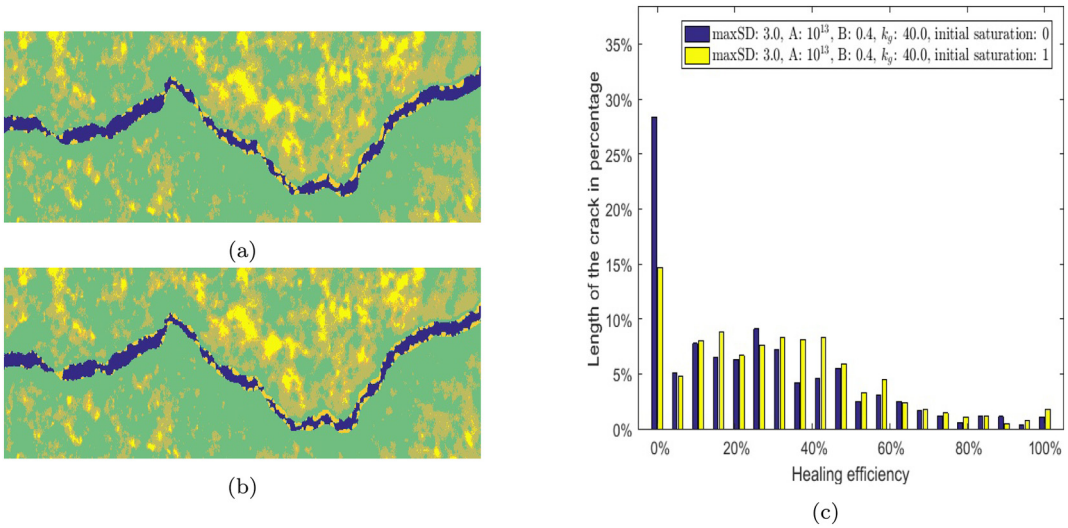

Fig. 7. The impacts of initial saturation condition: (a) Initialised with water, (b) initialised with saturated solution, (c) statistic analysis.

Table 5
The parameters of validation simulation.

maxSD (Unit: 1)	*A* (Unit: $m^{-3}s^{-1}$)	*B* (Unit: 1)	k_g (Unit: $kg\,m^{-2}s^{-1}$)	Initial saturated
3	10^{12}	0.4	160	Yes

4. Results and discussion

To valid the self-healing model, the simulation is compared with two experiments, i.e., the autogenous self-healing experiments carried out by [19] and the experimental results by [14]. Based on the aforementioned parameters study, the parameters used in the simulation are given in Table 5.

The simulation results shown in Fig. 8a has similar filling pattern compared to the experiment in Fig. 8b [19]. The healing fraction distributions show similar trend in Fig. 8c, except for the efficiency between 5% and 20%. This may be attributed to the experimental method used in [19]. When the sample is very thin, the embedded crystal products on the crack edge are also highlighted under crossed-polarized filters of the light microscope. These crystals are sorted out in image analysis as healing products, even though they exist before the self-healing experiment.

The filling efficiency γ of the simulation is compared with the experiment data from [14]. Both results are normalized with Eq. (27) to the crack width w_{ref} 10 μm. The simulation at early age experiences low filling fractions, while it shows good agreements at later age with experiment from [14]. It may be attributed to the existing nucleation sites at the crack age. In the simulation, all the nucleus are formed independently according to nucleation probability distribution. However, the crack edge in the experiment with defects are prone to nucleation and growth [31]. Random seeding at initial condition may address this problem, because the hydration product can form around the seeds directly when the solution is saturated.

$$\gamma_{norm} = \gamma \cdot \frac{w_{crack}}{w_{ref}} \tag{27}$$

Generally, both simulation and experiment show that the crack can be blocked efficiently with limited healing product, which may lead to lower effective diffusion coefficient of the cracked sample. A following research is proposed to evaluate the self-healing effect, e.g., the regaining of transport and mechanical properties.

5. Conclusion

The self-healing effect due to further hydration is simulated, taking into account the dissolution of unhydrated cement particle, ions transport, and nucleation and growth of hydration product. In this mesoscale model, the dissolved ions are considered as a single solute and the phase of individual product is not separated. This also reduces the computational burdens in the simulation when the physical length of the crack reaches to thousands micrometers. The model simulates not only the healing efficiency but also the geometry change due to self-healing. The changing geometry can be used to simulate the chloride migration test, in order to obtain the effective diffusion coefficients and chloride profiles.

The dissolution rate of unhydrated cement is calculated, taking into account the transition thickness. Lattice Boltzmann Method is used to simulate the dissolved cement. The nucleation probability distribution is employed to quantify and locate the formation of nucleus. The thermodynamics is used to calculate the growth rate of the nucleus.

The simulation shows good agreements with the experiments, in

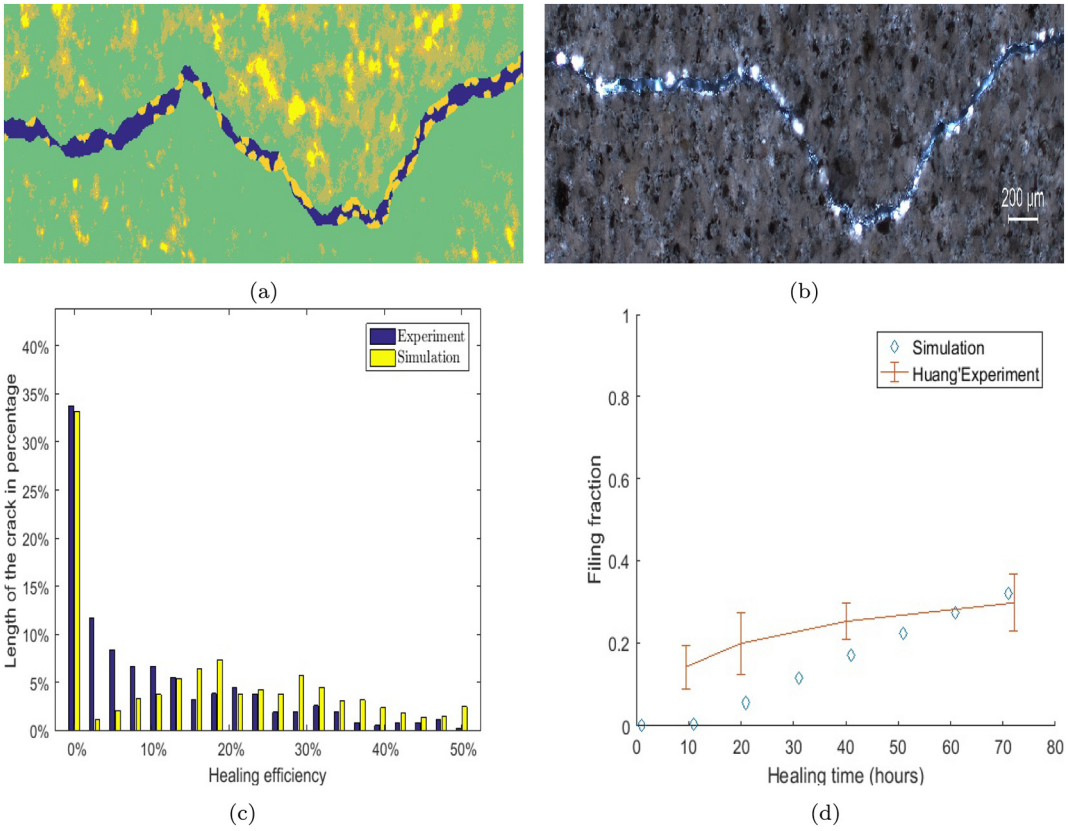

Fig. 8. Comparison of simulation and experiment results: (a) simulation 3 days: healing product is highlighted in the crack; (b) experiment 3 days: healing product is highlighted in white with crossed-polarized filters [19]; (c) healing product distribution analysis of simulation and experiment; (d) comparison of filling fraction between simulation and result from [14].

terms of healing patterns and healing product distributions. A following study will be proposed to evaluate the self-healing effects, e.g.,regaining of mechanical and transport properties of cementitious materials.

Declaration of Competing Interest

The authors declare that they have no known competing financial interests or personal relationships that could have appeared to influence the work reported in this paper.

Acknowledgments

The authors would like to thank the China Scholarship Council (CSC) for the financial support for this work.

References

[1] M.G.M. Wu, B. Johannesson, A review: self-healing in cementitious materials and engineered cementitious composite as a self-healing material, Construct. Build. Mater. 28 (2012) 571–583.
[2] N. Hearn, C.T. Morley, Self-sealing property of concrete-experimental evidence, Mater. Struct. 30 (7) (1997) 404–411.
[3] N. Hearn, Self-sealing, autogenous healing and continued hydration: what is the difference? Mater. Struct. 31 (8) (1998) 563–567.
[4] K. van Breguel, Is there a market for self-healing cement-based materials, Proceedings of the First International Conference on Self-healing Materials, Noordwijk aan zee, the Netherlands, 2007.
[5] G. Hyde, W. Smith, Results of experiments made to determine the permeability of cements and cement mortars, J. Frankl. Inst. 128 (3) (1889) 199–207.
[6] WH Glanville, The permeability of portland cement concrete, Build. Res. Tech. Pap. 3 (1931) 1–61.
[7] E. Schlangen, Fracture mechanics, CT5146 Lecture Notes, Delft University of Technology, 2007.
[8] C. Edvardsen, Water permeability and autogenous healing of cracks in concrete, ACI Mater. J. 96 (4) (1999) 448–454.
[9] Y. Yang, M.D. Lepech, E.-H. Yang, V.C. Li, Autogenous healing of engineered cementitious composites under wet-dry cycles, Cem. Concr. Res. 39 (5) (2009) 382–390.
[10] Y. Zhu, Y. Yang, Y. Yao, Autogenous self-healing of engineered cementitious composites under freeze-thaw cycles, Construct. Build. Mater. 34 (2012) 522–530.
[11] A. Suleiman, M. Nehdi, Effect of environmental exposure on autogenous self-healing of cracked cement-based materials, Cem. Concr. Res. 111 (2018) 197–208.
[12] K. Tomczak, J. Jakubowski, The effects of age, cement content, and healing time on the self-healing ability of high-strength concrete, Construct. Build. Mater. 187 (2018) 149–159.
[13] H. Huang, G. Ye, Simulation of self-healing by further hydration in cementitious materials, Cem. Concr. Compos. 34 (4) (2012) 460–467.
[14] H. Huang, G. Ye, D. Damidot, Characterization and quantification of self-healing behaviors of microcracks due to further hydration in cement paste, Cem. Concr. Res. 52 (2013) 71–81.
[15] A.S. Chitez, A.D. Jefferson, A coupled thermo-hygro-chemical model for characterising autogenous healing in ordinary cementitious materials, Cem. Concr. Res. 88 (2016) 184–197.
[16] A. Aliko-Benitez, M. Doblare, J. Sanz-Herrera, Chemical-diffusive modeling of the self-healing behavior in concrete, Int. J. Solids Struct. 69–70 (2015) 392–402.
[17] K. van Breugel, Simulation of Hydration and Formation of Structure in Hardening Cement-based Materials, Ph.D. Thesis Delft University of Technology, 1991.
[18] J. van der Lee, L. de Windt, CHESS, accessed: Oct 2018 http://chess.geosciences.mines-paristech.fr/.
[19] J. Chen, X. Liu, G. Ye, Quantification of the filling of microcracks due to autogenous self-healing in cement paste, Proceedings of International RILEM Conference on Materials, Systems and Structures in Civil Engineering Conference segment on Service Life of Cement-based Materials and Structures, 2016, pp. 745–754.
[20] T.C. Powers, Structure and physical properties of hardened Portland cement paste, J. Am. Ceram. Soc. 41 (1) (1958) 1–6.
[21] H. Huang, Thermodynamics of Autogenous Self-healing in Cementitious Materials, Ph.D. thesis Delft University of Technology, 2014.
[22] S. Bejaoui, B. Bary, Modeling of the link between microstructure and effective diffusivity of cement pastes using a simplified composite model, Cem. Concr. Res. 37 (3) (2007) 469âĂŞ480.
[23] R. Parsons, Self-diffusion in electrolyte solutions. Physical sciences data no. 36, J. Electroanal. Chem. Interfacial Electrochem. 264 (1–2) (1989) 307–308.
[24] H.M. Jennings, A model for the microstructure of calcium silicate hydrate in cement paste, Cem. Concr. Res. 30 (1) (2000) 101–116.
[25] X. You-Sheng, Z. Yi-Jun, H. Guo-Xiang, Lattice Boltzmann method for diffusion-reaction-transport processes in heterogeneous porous media, Chin. Phys. Lett. 21 (7) (2004) 1298.
[26] E. Walther, R. Bennacer, C. Desa, Lattice Boltzmann method applied to diffusion in restructured heterogeneous media, Defect and Diffusion Forum, vol. 354, Trans Tech Publ, 2014, pp. 237–242.
[27] D. Gao, Z. Chen, L. Chen, D. Zhang, A modified lattice Boltzmann model for conjugate heat transfer in porous media, Int. J. Heat Mass Transf. 105 (2017) 673–683.
[28] A.L. Greer, K. Kelton, Nucleation in Condensed Matter: Applications in Materials and Biology, Gardners Books, 2010.
[29] S. Jiang, J.H.T. Horst, Crystal nucleation rates from probability distributions of induction times, Cryst. Growth Des. 11 (1) (2011) 256–261.
[30] S. Srisanga, A.E. Flood, S.C. Galbraith, S. Rugmai, S. Soontaranon, J. Ulrich, Crystal growth rate dispersion versus size-dependent crystal growth: appropriate modeling for crystallization processes, Cryst. Growth Des. 15 (5) (2015) 2330–2336.
[31] J. Elam, C. Nelson, R. Grubbs, S. George, Nucleation and growth during tungsten atomic layer deposition on SiO_2 surfaces, Thin Solid Films 386 (1) (2001) 41–52.